Assembly dynamics of supramolecular protein-DNA complexes studied by single-molecule fluorescence microscopy

Stratmann, Sarah

Chapter 4

The innate immune sensor IFI16 recognizes foreign DNA in the nucleus by scanning along the duplex

Sarah Stratmann*, Seamus Morrone,* Antoine van Oijen, Jungsan Sohn

*equal contribution

eLife, 2015 Dec 16, Volume 4

The ability to recognize foreign double-stranded (ds)DNA of pathogenic origin in the intracellular environment is an essential defense mechanism of the human innate immune system. However, the molecular mechanisms underlying distinction between foreign DNA and host genomic material inside the nucleus are not understood. By combining biochemical assays and single-molecule techniques, we show that the nuclear innate immune sensor IFI16 one-dimensionally tracks long stretches of exposed foreign dsDNA to assemble into supramolecular signaling platforms. We also demonstrate that nucleosomes represent barriers that prevent IFI16 from targeting host DNA by directly interfering with these one-dimensional movements. This unique scanning-assisted assembly mechanism allows IFI16 to distinguish friend from foe and assemble into oligomers efficiently and selectively on foreign DNA.

4.1 Introduction

The host innate immune system detects infection by directly recognizing molecular signatures associated with pathogens (1, 2). Remarkably, such signatures include universal building blocks of all life, such as DNA and RNA (3-5). In the cytoplasm, the immune system relies on the absence of endogenous DNA, and thus marks all detected DNA as "foreign" (nonself) (4, 5). However, DNA viruses often evade the cytosolic detection machineries, as their genomes are not exposed until reaching the nucleus (4, 5). The host counters this infection strategy in the nucleus by directly assembling supramolecular signaling platforms that trigger inflammatory responses on invading foreign DNA, but not on its own genomic material (6-8). Although key players that target foreign dsDNA in the host nucleus have been identified (4, 5), the molecular mechanisms by which these sensors distinguish self from nonself dsDNA remain unknown.

The interferon-inducible protein 16 (IFI16) is a key innate immune sensor that detects foreign dsDNA and uses it as a scaffold to assemble supra-molecular signaling platforms in both the host nucleus and cytoplasm (6-10) (Figure 1A). IFI16 plays a central role in defense against a number of pathogens (e.g., herpes simplex virus-1) (6-10). On the other hand, persistent IFI16 signaling is associated with autoimmunity (e.g. Sjögren's syndrome) (11-15). The molecular mechanisms by which IFI16 selectively targets foreign dsDNA remain unknown. To establish a functional signaling platform, IFI16 must overcome two challenges. First, individual IFI16 molecules must be able to locate one another on large pathogen genomes with sizes ranging from 105 to 106 base pairs (bps). Second and more importantly, this assembly mechanism can only take place on foreign dsDNA and must be inhibited on host dsDNA (Figure 1A). Here, we report the observation of a unifying molecular mechanism that explains how IFI16 resolves these central issues in initiating its foreign-dsDNA sensing pathways.

4.2 Results and Discussion

To identify the mechanisms underlying assembly of IFI16 signaling platforms on DNA, we monitored the oligomerization kinetics of FRET donor and acceptor labeled IFI16 on naked dsDNA (FRET: fluorescence resonance energy transfer; Figure 1B and Supplementary Figure 1). Previous work demonstrated the existence of such oligomers and reported on their equilibrium binding properties, but did not provide insights into the assembly mechanisms (16). Using various dsDNA fragment sizes present in excess, we observe that the assembly rate increased non-linearly and by 50-fold from 60 to 200 bps dsDNA, above which it stayed constant (up to 600 bps; Figures 1B, 1C). With a dsDNA-binding footprint of ~15 bp for one IFI16 (16), our results indicate that about four copies are required to initiate assembly, and about ten IFI16 molecules are required for optimal oligomeric assembly (Figure 1C). Further, the assembly rate constants scaled linearly with the IFI16 concentration for all measured DNA lengths (Supplementary Figure 1 and Supplementary Table 1), indicating that a purely cooperative assembly mechanism is unlikely. In line with this observation, previous work reported relatively small contributions of cooperativity in oligomerization with Hill constants near 2 for DNA substrates up to 2000 bp (16).

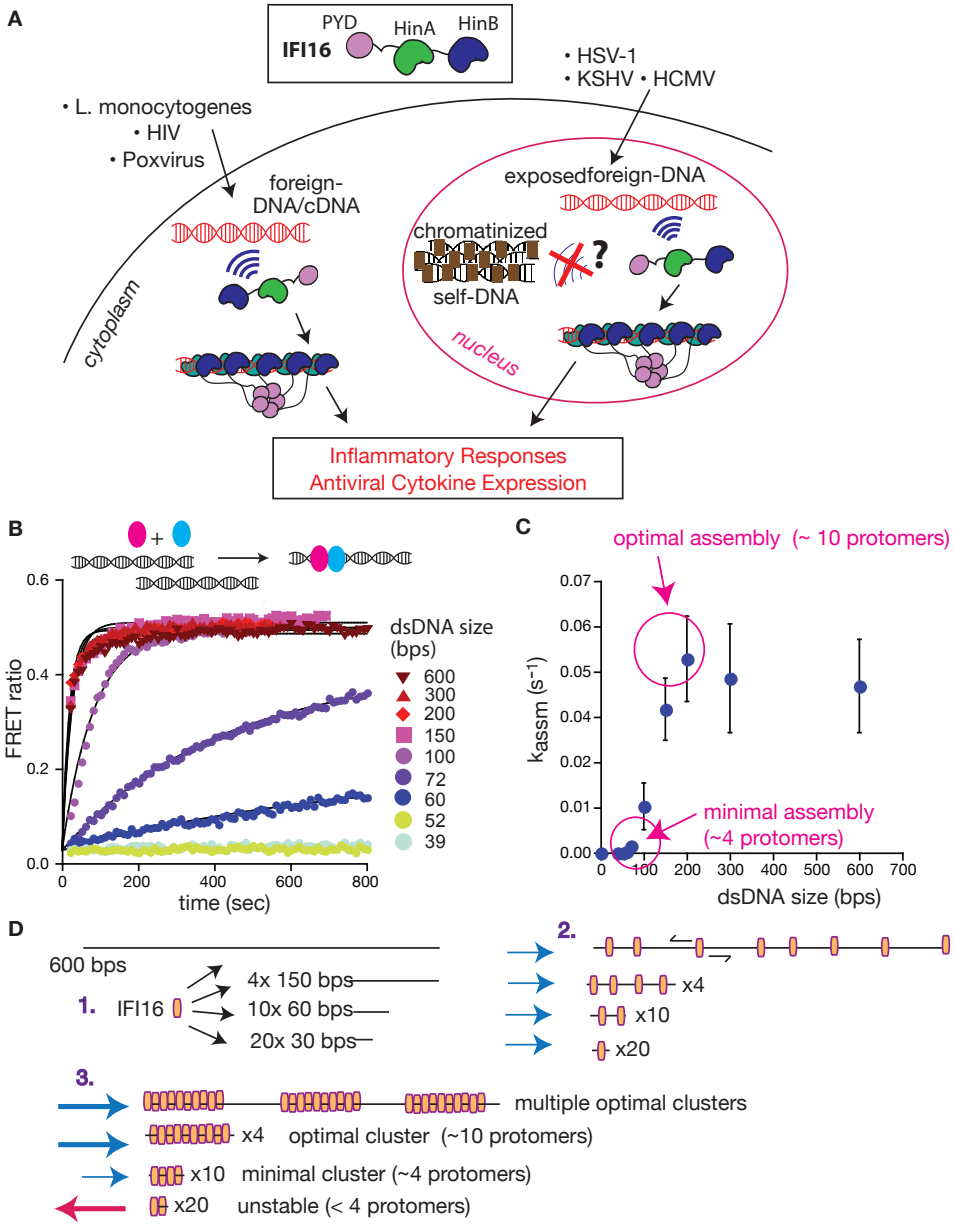

Figure 1: IFI16 assembles faster on longer dsDNA. **A)** Top: IFI16 is composed of three functional domains flanked by unstructured linkers, namely one pyrin domain (PYD) and two dsDNA-binding Hin domains (HinA and HinB; Hin: hematopoietic interferon inducible nuclear antigen). Bottom: IFI16 detects foreign dsDNA from invading pathogens in both host nucleus and cytoplasm. **B)** Top: a cartoon scheme for FRET experiments. The two differentially colored ovals represent fluorescently (Dylight-550 and Dylight-650) labeled IFI16. Bottom: The time-dependent changes in the emission ratio between FRET donor and acceptor labeled IFI16 (50 nM) were monitored at 33 μg/ml of each dsDNA (e.g. 6-fold higher than the dissociation constant for 39-bp dsDNA (16)). Lines are fits to a first-order

exponential equation (see Suppl. Fig. 1 for 25 nM protein). All shown representative experiments were performed at least three times. **C)** A plot of observed assembly rates (kassms) vs. dsDNA-sizes (see also Suppl. Table 1). **D)** 1D-diffusion assisted assembly mechanism can explain the observed assembly profile of IFI16. 1. At the same mass-concentrations, the number of individual dsDNA fragments present in each assay is inversely proportional to the length of dsDNA. 2. Individual IFI16 molecules initially bind dsDNA at random positions and diffuse one-dimensionally while searching for other respective protomers; the number of IFI16 residing on the same dsDNA fragment should be proportional to the length of dsDNA (e.g. there are 4 times more individual 150-bp fragments than 600-bp fragments) 3. IFI16 fails to assemble intoan oligomer on dsDNA shorter than 60 bp (indicated by a red arrow pointing left). The saturating rates can be explained if the final FRET signals arise from formation of distinctoptimal oligomers.

Our ensemble-averaged, solution-phase observations of the faster assembly on longer dsDNA suggest a model in which IFI16 scans along dsDNA to increase the probability of encountering other IFI16 molecules (Figure 1D). To directly test such a mechanism, we used single-molecule fluorescence imaging to track the movements of individual Cy5-labeled IFI16 molecules on stretched, double-sided attached λ-phage dsDNA (λdsDNA; 48.5 kbps) (Figure 2A). Figure 2B shows that individual IFI16 molecules one-dimensionally (1D) diffuse on λdsDNA while bound for several seconds. The diffusion coefficient of IFI16 increased with ionic strength, indicating that IFI16 does not maintain a continuous electrostatic interaction with the dsDNA backbone, but instead moves along the λdsDNA scaffold by executing microscopically small steps (17) (Figure 2B and Suppl. Figure 2). An IFI16 construct lacking the oligomerizing PYD (IFI16HinAB; see also Figure 1A) showed similar diffusional properties, suggesting that the dsDNA-binding HIN200 domains are responsible for 1D diffusion. Upon applying higher concentrations of IFI16 with a constant supply of proteins into our flow cell, we observed a gradual formation of distinct, immobile clusters along λdsDNA (Figure 2C and Suppl. Figure 3). Over time, we also observed an increase in the number of molecules per cluster and a concomitant decrease in the diffusion coefficient (Figures 2C, 2D). We analyzed the impact of flow on the diffusion coefficient and diffusion bias and found it to be not significant for cluster formation (Suppl. Figure 5). Single-molecule intensity analysis revealed that the lower limit of the number of IFI16 molecules found in immobile clusters is equivalent to eight protomers (Figure 2D and Suppl. Figure 4), which also corroborate the optimal complex (ten protomers) suggested from Figure 1C. Furthermore, individual IFI16 molecules either formed new clusters or joined other clusters in a stochastic manner, and the immobile clusters formed faster with higher IFI16 concentrations (Figure 2E). The rate of addition of IFI16 molecules to clusters is independent on the size of the existing cluster, confirming the absence of strong cooperativity in assembly (Figure 2C; bottom panel).

The 1D diffusion of IFI16 on dsDNA explains why the assembly rates increase with the DNA length in the bulk experiments (Figure 1C). With the longer dsDNA acting as an antenna, it allows binding of more IFI16 while 1D diffusion facilitates dynamic association (Figure 1D). The saturation of the assembly rate (Figure 1C) can be explained by the square dependence of the diffusional search time on length: at a sufficiently long dsDNA length, the dissociation rate of an individual IFI16 will be faster than the time needed to scan along the entire length of the DNA. In addition, longer DNA substrates work no longer as antennae, but as traps, since individual IFI16 molecules are farther apart and thus less likely to encounter one another (18-20). Overall, the results of our bulk and single-molecule experiments are consistent

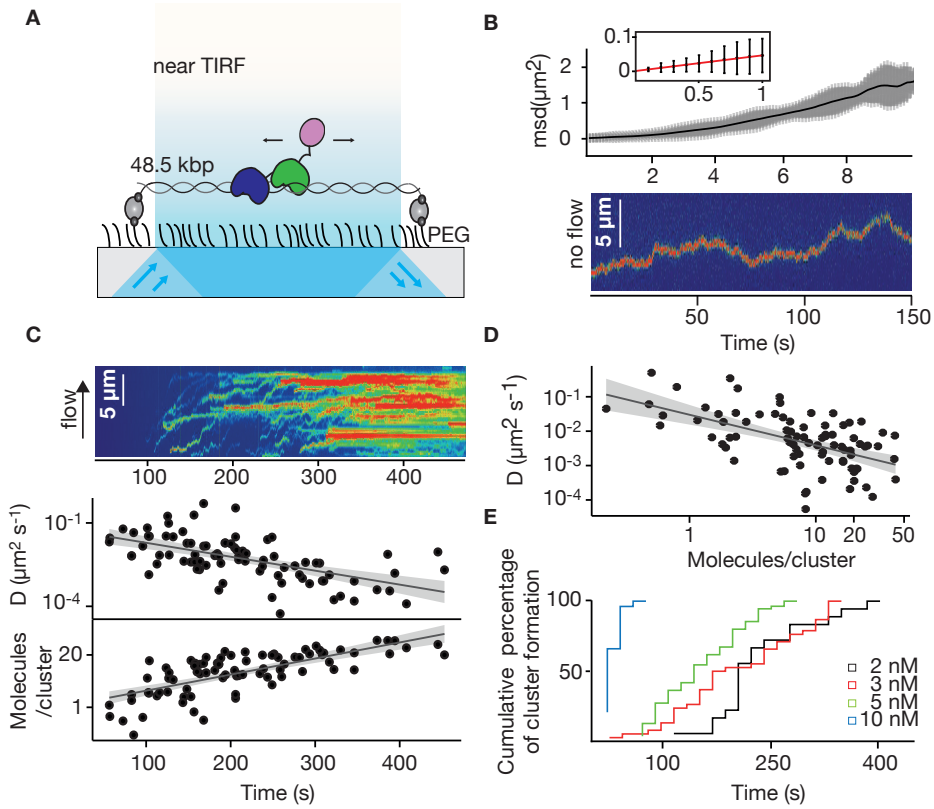

Figure 2: IFI16 scans dsDNA. **A)** Illustration of the TIRF setup. λdsDNA is anchored to the pegylated coverslip surface by either one or two biotinylated oligonucleotide linkers. Single-biotinylated λdsDNA is constantly stretched by flow during measurements and used for the clustering and nucleosome experiments, whereas double-biotinylated λdsDNA is stably attached whilst being stretched and used without flow for single-molecule diffusion coefficient analysis. **B)** Double-biotinylated λdsDNA is anchored to the surface and Cy5-labeled IFI16 molecules (800 pM) are visualized in near TIRF while bound to DNA. Top: Mean-square displacement (msd) trajectories are fitted within their linear regime to calculate the 1D-diffusion coefficient. Bottom: A sample kymograph of a single molecule stably bound for tens of second to DNA and exerting Brownian motion. **C)** Elevated IFI16 concentrations result in clustering along λdsDNA. Top: A sample kymograph of multiple IFI16 molecules (3 nM) diffusing along λdsDNA. IFI16 molecules display a net motion along the flow direction. Bottom: Time-resolved clustering is accompanied by a decrease in diffusion coefficients and increase in the number of molecules per cluster. **D)** The diffusion coefficient inversely correlates with the number of IFI16 per cluster, resulting in immobile, stable oligomers. **E)** Cluster formation is IFI16-concentration dependent.

with the dsDNA-size dependent binding *in vitro* (16), which also correlates with the IFI16-induced inflammatory responses *in vivo* (9). Thus, we propose that the 1D-diffusion mediated assembly plays a key role in regulating the overall IFI16-mediated immune responses.

It has long been speculated that chromatinization acts as the key feature that allows IFI16 to distinguish host from foreign DNA in the nucleus (7, 8, 10, 21-23); IFI16 oligomerizes on exposed invading foreign-dsDNA before it becomes hetero-chromatinized. Previous *in*

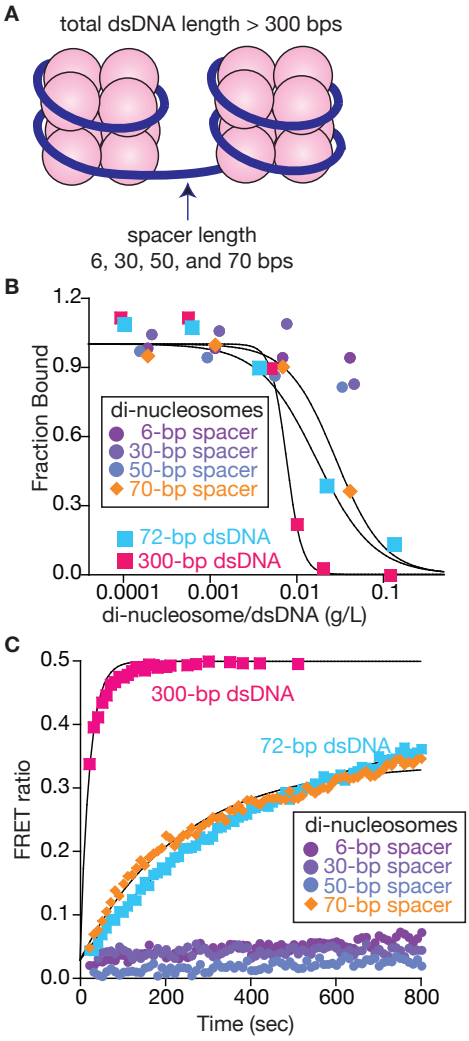

Figure 3: Nucleosomes inhibit oligomerization. **A)** A cartoon of di-nucleosome constructs with varying double stranded DNA spacers. **B)** Competition binding assays using IFI16 bound FAM-labeled 70-bp dsDNA against various di-nucleosomes and naked dsDNA. The lines are fits to: $1/(1+([DNA_{competitor}]/IC_{50})^{Hill\ constant})$, where IC_{50} indicates the concentration of competitor at 50% efficiency. The mass-concentration of each competitor was calculated using dsDNA, but not histones. **C)** The time-dependent changes in the emission ratio between the FRET donor and acceptor labeled IFI16 (50 nM) were monitored at 33 μg/ml of each nucleosome or naked dsDNA. The lines are fits to a first-order exponential equation.

vivo work demonstrated that transfected chromatinized SV40 DNA is able to evade IFI16 oligomerization and downstream responses (22). Nevertheless, the molecular mechanism by which IFI16 could use chromatinization to distinguish self from nonself has yet to be identified. To directly address this issue, we first used a competition-binding assay to investigate how IFI16 interacts with dsDNA fragments containing two nucleosomes with varying spacer sizes (6, 30, 50, and 70 bps; Figure 3A and Suppl. Figure 6A). Here, di-nucleosomes with 6-, 30-, and 50-bp spacer failed to compete against IFI16-bound FAM-labeled 70-bp dsDNA, (Figure 3B). On the other hand, the di-nucleosome with 70-bp spacer competed similarly as 70-bp naked dsDNA, but significantly more weakly than naked 300-bp dsDNA (Figure 3B). In FRET assembly assays, di-nucleosomes with spacers shorter than 70-bp failed to support assembly (Figure 3C), consistent with our FRET kinetics assays using naked dsDNA (Figure

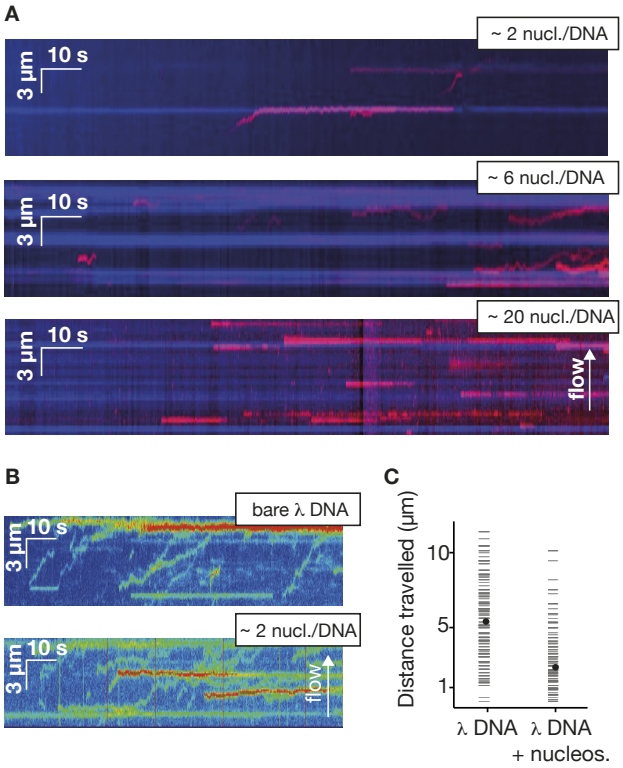

Figure 4: Nucleosomes inhibit 1D-diffusion. **A)** Kymographs of Cy5-labeled IFI16 (magenta) binding to λdsDNA with varying numbers of nucleosomes tagged with anti-H4-Atto488 (blue). The number of nucleosomes per λdsDNA were estimated by quantifying IFI16 clustering sites for the lowest nucleosome/λdsDNA ratio (Suppl. Fig. 7B), yielding ~2 nucleosomes/ λdsDNA. At low nucleosome concentrations (~2 to 6 nucleosomes/DNA), IFI16 binds to λdsDNA and diffuses with the flow direction, until encountering a nucleosome. At higher concentrations (~20 nucleosomes per λdsDNA), individual IFI16 show only very short diffusive movements upon binding. **B)** On naked λdsDNA, IFI16 travels with the flow to the free tip (top), whereas it oligomerizes along the path on nucleosome-loaded λdsDNA (bottom). **C)** The overall travel distance of single IFI16 on nucleosome-loaded λdsDNA is reduced compared to bare λdsDNA (nucleosomal λdsDNA: N=167, bare λdsDNA: N=141).

1B). The 70-bp spacer di-nucleosome supported oligomerization of IFI16; however, the assembly kinetics was again similar to that of naked 70-bp dsDNA, but not that of naked 300-bp dsDNA (Figure 3C). Taken together, these results show that efficient IFI16 cluster formation requires a minimal length of 50-70 base pairs of exposed dsDNA. Considering that the size of dsDNA linker between two nucleosomes is about 20 to 30 bps in mammals (24), these results directly support the hypothesis that chromatinization is a key deterrent for preventing the assembly of IFI16 signaling platforms on self-dsDNA.

To test whether the inhibitory effect of chromatin directly arises by interfering with the 1D diffusion of IFI16, we visualized the movement of individual IFI16 molecules on DNA with

nucleosomes. We introduced randomly localized nucleosomes in λdsDNA using recombinant human histone octamers and tagged nucleosome positions with fluorescent antibodies against the N-terminal tail of histone H4 (Suppl. Figure 6B). The application of hydrodynamic flow resulted in the single IFI16 molecules being pushed to one direction and clustering at nucleosomal sites on λdsDNA, unable to overcome the octamers by diffusion (Figure 4A and Suppl. Figure 7C). Without the antibody, the motion of IFI16 was still confined, whereas for bare λdsDNA, IFI16 moved with a high processivity along the entire strand (Figures 4B, 4C, and Suppl. Figure 7A, B). These observations are consistent with the bulk experiments (Figure 3), and confirm that nucleosomes directly restrict the 1D diffusion of IFI16 and consequently limit the assembly of IFI16 signaling platforms on dsDNA.

The molecular mechanism by which innate immune sensors distinguish self from foreign dsDNA in the host nucleus has been a major unresolved question in innate immunology (7, 8, 10, 21-23, 25). The oligomerization of IFI16 on under-chromatinized foreign DNA plays a key role not only in initiating inflammatory and antiviral responses, (8, 10, 26), but also in regulating the hetero-chromatinization and silencing of viral dsDNA (22, 23). By using time-resolved bulk and single-molecule fluorescence assays, we demonstrate here that IFI16 one-dimensionally scans along exposed dsDNA to assemble into distinct clusters and that chromatinization is sufficient to inhibit IFI16 from targeting host dsDNA for assembly. *In vivo*, this 1D scanning mechanism allows a limited number of IFI16 molecules to allocate each other on large genomes of invading pathogens. In combination with 3D sampling of binding sites on a collapsed DNA molecule, this process optimizes the oligomerization and downstream signaling time. While the clustering on dsDNA presents a tempting explanation for the role of IFI16 in viral gene silencing, future *in vivo* experiments await to test this. IFI16 belongs to the family of AIM2-like receptors, which include other nuclear and cytosolic foreign dsDNA-sensors. It will be interesting to determine whether and how these other related sensors use exposed dsDNA as a 1D "digital ruler" to regulate their signaling platform assembly. This family of sensors is implicated in a number of autoimmune disorders (11-15); how regulation of assembly is disrupted may provide insights into these afflictions.

4.3 Materials and Methods

Protein Expression and Purification

Human full-length IFI16 and IFI16HinAB were cloned and expressed using *E. coli* T7 express cells (NEB) as a C-terminally His6-tagged protein as described in Morrone et al. (16).

DNA Ligand Preparation

dsDNA shorter than 90-bp were obtained from Integrated DNA Technologies (IDT) as described in Morrone et al. (16). The complementary strands were dissolved and mixed in 1:1

molar ratio, melted at 95°C for 10min, and the temperature was lowered to 25°C at a rate of 1°C/min. Ligands of greater length were obtained by polymerase-chain reaction (PCR) using the Maltose Binding Protein fusion tag cloning sequence as template and primers of appropriate sequence for a final length as indicated in the paper. Plasmids containing the Widom-601/603 sequence with indicated linker lengths were a kind gift of Dr. Gregory Bowman. The nucleosomal DNA was obtained by PCR from these constructs with appropriate primers. All substrates were gel-purified.

Fluorescent Labeling

DyLight-550, DyLight-650, or Cy5 fluorophore was incorporated to IFI16 using maleimide chemistry (purchased from Thermo Scientific and Invitrogen) and was performed as described in Morrone et al. (16). The label to protein ratio was ~ 1:1. Fluorescein-labeled dsDNA72 was obtained from IDT.

Octamer Refolding and Nucleosome Reconstitution

Lyophylized Xenopus laevis histones H1A, H2A, H3, and H4 were a kind gift of Dr. Cynthia Wolberger. Octamer refolding and nucleosome reconstitution was performed as described in Luger et al. (27), at a 2:1 molar ratio of octamer:DNA. An agarose gel of reconstituted nucleosomes is shown in Suppl. Figure 6A.

Bulk Biochemical Assays

All absorption, fluorescence anisotropy, and fluorescence excitation/emission experiments were performed in a Tecan Infinite M1000. All experiments were performed at least three times and the fits to data were generated by Kaleidagraph software (synergy).

Competition Binding Assays

All reactions were performed in 40 mM HEPES pH 7.4, 160 mM KCl, 5 % glycerol, 1 mM EDTA, 0.1 % triton-X-100, 5 mM DTT (Reaction Buffer). 300 nM IFI16 and 4.5 nM fluorescein-labeled dsVACV72 were incubated together at room temperature for 20 min. Increasing concentrations of competing DNA were added to the reaction to a final concentration of 100 nM IFI16 and 1.5 nM dsVACV72, and the changes in fluorescence anisotropy were recorded as indicated in Morrone et al. (16).

FRET Time Dependence Assays

All reactions were performed in Reaction Buffer. 66 μg/ml of each dsDNA or di-nucleosomes was placed in the plate wells, and the reaction was initiated by adding an equivalent volume of IFI16-550 and IFI16-650 (1:1 molar ratio) to the indicated final concentration. The dead

time between addition of IFI16 and the first measurement was 15-20s. The final dsDNA molar-concentrations are at least 6-fold higher than their determined binding constants by fluorescence anisotropy assays described in Morrone et al. (2014) (16), and the FRET ratio for each time point was calculated by dividing the acceptor emission (678 nm) by the donor emission (574 nm) (16).

Fluorescence microscopy assays

Microscope coverslips (Corning) were plasma-cleaned and activated with 100 mM KOH, silanized with 3-Aminopropyl-triethoxysilane in acetone and functionalized with PEG-NHS and biotin-PEG-NHS (Laysan-Bio) in sodium bicarbonate with a 1:3 mass ratio (28). Streptavidin (Sigma Aldrich) was used for anchoring the biotinylated DNA substrates to the coverslip surface. Flow channels were constructed with custom-made PDMS chips to obtain dimensions of 10 mm length, 100 μm height and 1 mm width, and connected to a syringe pump to allow constant flow during the measurements.

Single-molecule assays were performed in 40 mM HEPES (pH 7.4), 160 mM KCl, 1 mM EDTA, 2 mM DTT, 10 % glycerol, 0.1 % Triton-X100, 250 μg/ml BSA, 1 mM Trolox, 40 mM glucose, 250 nM glucose oxidase, 60 nM catalase, unless otherwise stated. All assays were performed at room temperature. We applied 100 nM YoPro-1 iodide (Life Technologies) at the end of the measurements to visualize the DNA substrates.

Reactions were illuminated with a 488-nm and 641-nm laser (Coherent) and images were acquired with an EMCCD camera (Hamamatsu). We used MetaVue imaging software (Molecular Devices) for data acquisition and ImageJ and R for analysis.

λ-DNA templates for microscopy

Lambda-DNA (New England Biolabs) was biotinylated at one or both ends by ligation of the respective complementary biotinylated oligos according to Tanner et al. (28) (oligo sequences are given in Supplementary Table 2; purchased from IDT). Single-biotinylated DNA templates were stretched by constant flow (20 μl/min) throughout the experiments (IFI16 clustering and nucleosome assays). Double-biotinylated DNA templates were applied to the flow cell at high flow velocity (100 μl/min). This allowed binding of the DNA to two biotin moieties, while the DNA was stretched. Free DNA was washed out, IFI16 applied to the flow cell, and flow was then stopped for acquisition of the single molecule diffusion traces.

To reconstitute nucleosomes, recombinant histone H2A/H2B dimers and H3/H4 tetramers (New England Biolabs) were assembled on biotin-λ-DNA and biotin-601 sequence (Epicypher) by salt gradient dialysis (2 M to 0.3 mM NaCl in 5 steps, each step with an incubation time of at least 2 h) in 10 mM Tris/HCl, pH 7.4, 0.1 mM EDTA, 0.5 mM DTT. We tested nucleosome reconstitution by an EMSA assay on digested λ-DNA (Suppl. Figure 6B). For this, we generated DNA fragments by digestion with EcoRI (NEB), purified them (Qiagen DNA spin columns) and reconstituted nucleosomes in the concentration ratios that we also used for full-length λ-DNA.

Single molecule co-localization of IFI16 with nucleosomes tagged with antibodies

Antibodies against human histone H4 and H2B were chosen to target the N-terminal histone tails (Santa Cruz, sc-8657 and sc-8650), and labeled with Atto488-NHS (Life technologies) in PBS at pH 7.0. Labeled antibodies were negatively tested against bare DNA and Ifi16 clusters in the microscopy assay, and showed high specificity for nucleosomal DNA preparations only.

λ-DNA templates, loaded with nucleosomes and tagged with anti-H4, were constantly stretched in the flow channel. Ifi16 co-localized strongly with the nucleosome signal (movie 3). In contrast, biotinylated 601-sequence prepared with nucleosomes and tagged with anti-H4-Atto488, hardly showed co-localization with Ifi16, indicating, that there is not sufficient exposed dsDNA available for binding (Suppl. Figure 7C).

Drift correction

For the clustering experiments, we applied a flow of 0.02 ml/min to our flow cell design of 0.1 mm height and 1 mm width, giving a volumetric flux of 0.33 cm/s. We expect the DNA molecules to be on average 0.2 μm away from the surface (29), giving a velocity v_y at distance y and channel height h (30):

$$v_y = \frac{3}{2} v_{avg} \left(\frac{hy - y^2}{h^2/4} \right) = 40 \text{ [μm/s]}, \qquad \text{with } v_{avg} = \frac{2}{3} v_{max}$$

The Stokes drag force that acts on the DNA and bound IFI16 molecules is then described by

$$F = 6\pi\eta r v_y \left(1 + \frac{9r}{16y}\right) = 1.5 \text{ [fN]},$$

with viscosity η, radius r and distance y.

We can define this force within the diffusion coefficient D by using the drift velocity v, calculated from single-molecule trajectories, with displacement Δx_i taking place over time Δt_i (31):

$$D = \frac{1}{2}\left(\frac{1}{n}\sum_{i}^{n} \frac{(\Delta x_i - v\Delta t_i)^2}{\Delta t_i}\right),$$

$$\text{with } v = \frac{\sum_j^{all\ traj.} x_{j,final} - x_{j,initial}}{\sum_j^{all\ traj.} t_{j,final} - t_{j,initial}} \approx 0.127 \text{ [μm/s]}.$$

In order to evaluate the effect of flow on the clustering mechanism, we implemented a 1D-random walk Monte-Carlo simulation (Suppl. Figure 5). Here, we calculated the expected search time for two IFI16 molecules (with D=0.026 μm^2/s) to allocate each other on a λ-DNA molecule congested with a varying amount of other diffusing IFI16 molecules (10, 50, 100

molecules). As all particles are equal, we segmented the DNA according to the total number of molecules bound and calculated the effective distance between two particles by using the absolute distance modulo the segment length in order to take the periodic boundaries into account.

We allowed a maximum distance of 10 nm to consider two particles having met and dimerized. To simulate flow similar to our experimental conditions, to each random step the term vdt was added (The Python code is found in the online publication at the eLife website).

4.4 Supplementary data

Suppl. Table 1: dsDNA-mediated oligomerization rates of FRET-labeled IFI16. Each experiment was performed at least three times and errors were calculated by using the standard deviations.

dsDNA size (bps)	25 nM IFI16 (sec^{-1})	50 nM IFI16 (sec^{-1})
60	0.0004 ± 0.0002	0.0009 ± 0.0002
70	0.0008 ± 0.0002	0.0021 ± 0.0008
100	0.0052 ± 0.0008	0.012 ± 0.005
150	0.019 ± 0.004	0.037 ± 0.008
200	0.021 ± 0.007	0.049 ± 0.011
300	0.029 ± 0.008	0.045 ± 0.014
600	0.021 ± 0.008	0.043 ± 0.012

Suppl. Table 2: Oligonucleotides used in this study are listed below.

λ oligo 1	5'GGGCGGCGACCTGGACAGCAAGTTGGACAATCTC-GTTCTATCACTAATTCACTAATGCAGGGAGGATTTCA-GATATGGCA-3'
λ oligo 2	5'-biotin-A(16)GAGTACTGTACGATCTAGCATCAAT-CACAGGGTCAGGTTCGTTATTGTCCA-3'
λ oligo 3	5'-AGGTCGCCGCCCA(12)-biotin-3'
601-sequence	5'-biotin-ATCGAGAATCCCGGTGCCGAGGCCGCT-CAATTGGTCGT AGACAGCTCTAGCACCGCTTAAAC-GCACGTACGCGCTGTCCCCCGCGTTTTAACCGC-CAAGGGGATTACTCCCTAGTCTCCAGGCACGTGTCA-GATATATACATCCGAT

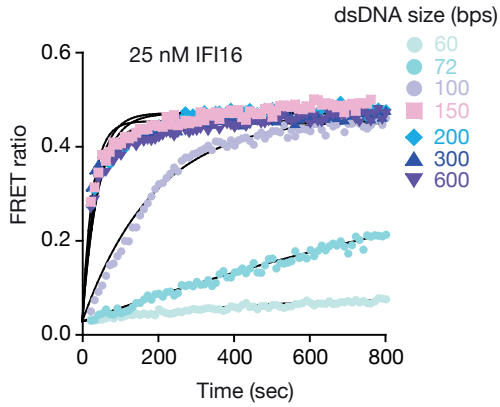

Suppl. Figure 1: FRET assembly assays using 25 nM donor and acceptor labeled IFI16 compared to 50 nM in Fig. 1B. Shown is a representative of three experiments and the calculated rates are listed in Suppl. Table 1.

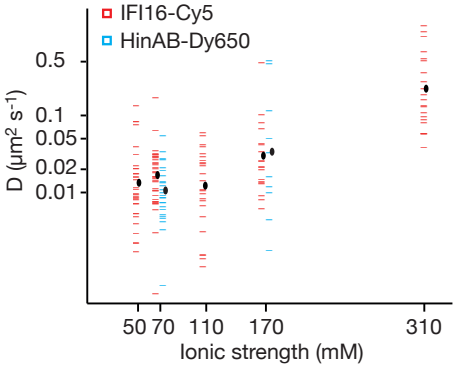

Suppl. Figure 2: Dependence of the diffusion coefficient of IFI16 and IFI-16HinAB mutant on salt concentration. (i) IFI16: The median of D increases from 0.017 to 0.18 $\mu m^2 s^{-1}$ with increasing ionic strength from 0.07 M to 0.31 M concomitant with decreasing binding times to DNA. (ii) HinAB: The median increases from 0.010 to 0.027 $\mu m^2 s^{-1}$ with increasing ionic strength from 0.07 M to 0.017 M.

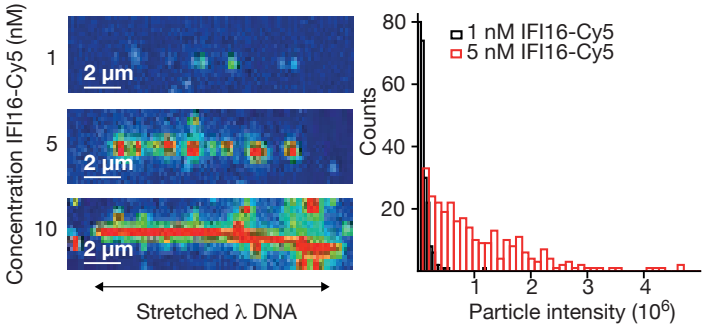

Suppl. Figure 3: (Left) Representative fluorescence images of IFI16-Cy5 on DNA molecules: Concentrations of 1 nM and 5 nM result in the resolution of single IFI16 molecules and distinguishable Ifi16 clusters, respectively, whereas a higher concentration of 10 nM eventually leads to DNA congestion with protein clusters or filaments. (Right) Intensities per particle are shown for 1 nM (single molecules) and 5 nM (clusters of IFI16). The mean particle intensity for single molecules serves as basis for calculating the number of IFI16 molecules within clusters (Suppl. Figure 4).

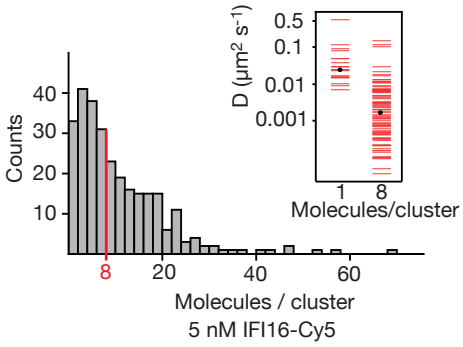

Suppl. Figure 4: Fluorescence data of 5 nM IFI16 are converted to cluster sizes. The mean cluster size amounts to 8 IFI16 molecules within a cluster. Clusters are almost immobile, represented by a significant reduction in the diffusion coefficient D compared to that of single molecules of IFI16.

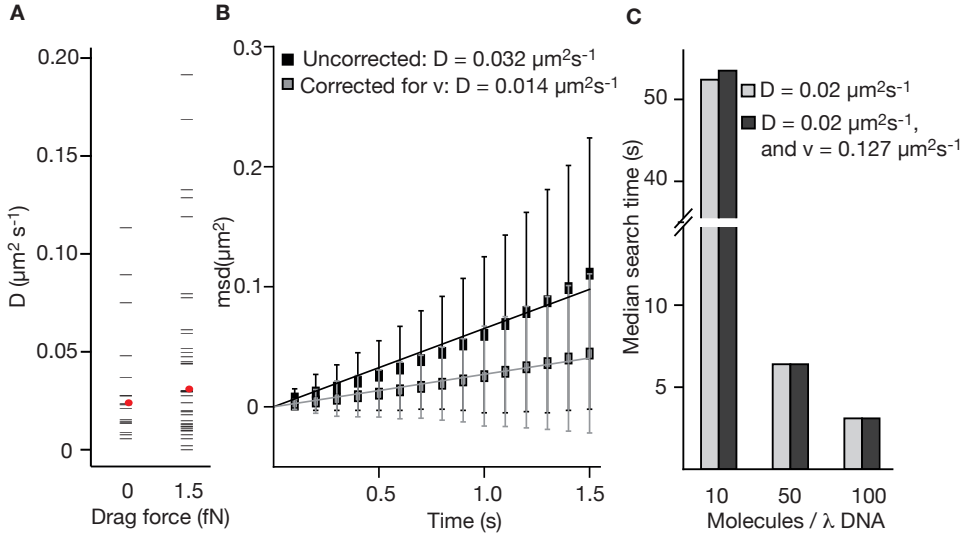

Suppl. Figure 5: A) Constant flow (20 µl/min) is applied for the clustering experiments with elevated IFI16 concentrations, corresponding to a drag force of 1-2 fN on the DNA substrate and bound IFI16 molecules. The median measured diffusion coefficient D for single molecules increases from 0.026 $\mu m^2 s^{-1}$ (no flow) to 0.031 $\mu m^2 s^{-1}$ (with flow). **B)** As described in the supplementary material, we calculated the drag velocity *v* on single molecules, with which we can define the effect of flow on D. Exemplarily shown here is a single diffusion trace, uncorrected and corrected for *v*. **C)** Monte-Carlo simulation of IFI16 dimerization on lambda DNA that is occupied by varying amounts of 1D-diffusing IFI16s. The presence of a drag velocity v does not significantly alter the median search time.

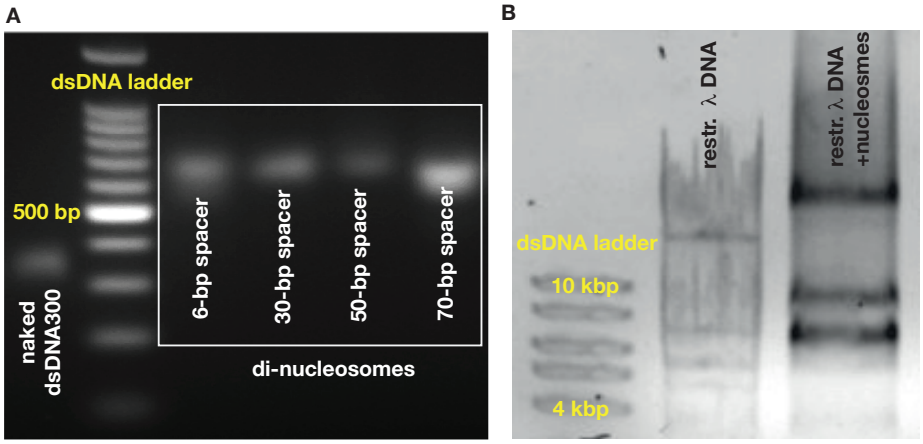

Suppl. Figure 6: Agarose gels with nucleosome preparations. **A)** Purified dinucleosomes for the bulk FRET assays. **B)** Reconstituted nucleosomes on restricted λdsDNA: EcoRI digestion generated l-DNA fragments of 21 kbp, 7.5 kbp, 5.8 kbp, 5.6 kbp, 4.8 kbp, and 3.5 kbp.

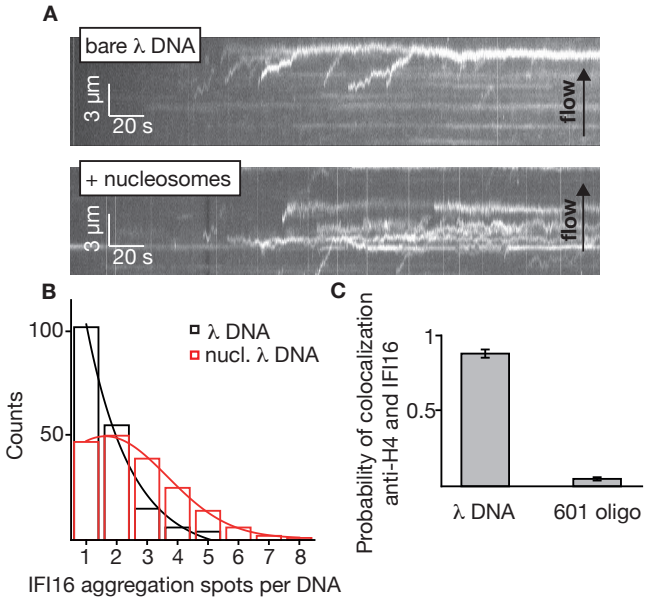

Suppl. Figure 7: A) Example kymographs of IFI16-Cy5 on bare λdsDNA with long processivities to the free DNA tip and on nucleosomal λdsDNA with reduced run lengths. **B)** Analysis of the number of IFI16 aggregation sites along DNA templates (including the free DNA tip) points to 1-3 nucleosomes per λdsDNA for the chosen reconstitution ratio DNA:histones, as it was used for run length measurements (Figs. 4B, 4C). **C)** Single-molecule co-localization probability of anti-H4-Atto488 with IFI16-Cy5 on nucleosomal biotin-λdsDNA and on biotin-601-nucleosomes (N=419 and 472, respectively). 601-nucleosomes do not provide sufficient exposed dsDNA for IFI16 binding, whereas on λdsDNA IFI16 molecules travel until encountering nucleosome obstacles.

4.5 References

1. C. A. Janeway, Jr., R. Medzhitov, Innate immune recognition. Annu Rev Immunol 20, 197 (2002).

2. R. Medzhitov, C. Janeway, Jr., Innate immune recognition: mechanisms and pathways. Immunological reviews 173, 89 (Feb, 2000).

3. R. Medzhitov, C. A. Janeway, Jr., Decoding the patterns of self and nonself by the innate immune system. Science 296, 298 (Apr 12, 2002).

4. M. H. Orzalli, D. M. Knipe, Cellular sensing of viral DNA and viral evasion mechanisms. Annu Rev Microbiol 68, 477 (2014).

5. S. R. Paludan, A. G. Bowie, Immune sensing of DNA. Immunity 38, 870 (May 23, 2013).

6. K. E. Johnson, L. Chikoti, B. Chandran, Herpes simplex virus 1 infection induces activation and subsequent inhibition of the IFI16 and NLRP3 inflammasomes. Journal of virology 87, 5005 (May, 2013).

7. T. Li, B. A. Diner, J. Chen, I. M. Cristea, Acetylation modulates cellular distribution and DNA sensing ability of interferon-inducible protein IFI16. Proc Natl Acad Sci U S A 109, 10558 (Jun 26, 2012).

8. N. Kerur et al., IFI16 acts as a nuclear pathogen sensor to induce the inflammasome in response to Kaposi Sarcoma-associated herpesvirus infection. Cell host & microbe 9, 363 (May 19, 2011).

9. L. Unterholzner et al., IFI16 is an innate immune sensor for intracellular DNA. Nature immunology 11, 997 (Nov, 2010).

10. M. H. Orzalli, N. A. DeLuca, D. M. Knipe, Nuclear IFI16 induction of IRF-3 signaling during herpesviral infection and degradation of IFI16 by the viral ICP0 protein. Proceedings of the National Academy of Sciences of the United States of America 109, E3008 (Oct 30, 2012).

11. M. Mondini et al., Role of the interferon-inducible gene IFI16 in the etiopathogenesis of systemic autoimmune disorders. Ann N Y Acad Sci 1110, 47 (Sep, 2007).

12. D. Choubey et al., Interferon-inducible p200-family proteins as novel sensors of cytoplasmic DNA: role in inflammation and autoimmunity. Journal of interferon & cytokine research : the official journal of the International Society for Interferon and Cytokine Research 30, 371 (Jun, 2010).

13. M. Mondini et al., The interferon-inducible HIN-200 gene family in apoptosis and inflammation: implication for autoimmunity. Autoimmunity 43, 226 (Apr, 2010).

14. F. Gugliesi et al., Nuclear DNA sensor IFI16 as circulating protein in autoimmune diseases is a signal of damage that impairs endothelial cells through high-affinity membrane binding. PloS one 8, e63045 (2013).

15. S. Smith, C. Jefferies, Role of DNA/RNA sensors and contribution to autoimmunity. Cytokine Growth Factor Rev, (Aug 15, 2014).

16. S. R. Morrone et al., Cooperative assembly of IFI16 filaments on dsDNA provides insights into host defense strategy. Proc Natl Acad Sci U S A 111, E62 (Jan 7, 2014).

17. P. C. Blainey, A. M. van Oijen, A. Banerjee, G. L. Verdine, X. S. Xie, A base-excision DNA-repair protein finds intrahelical lesion bases by fast sliding in contact with DNA. Proc Natl Acad Sci U S A 103, 5752 (Apr 11, 2006).

18. T. Hu, A. Y. Grosberg, B. I. Shklovskii, How proteins search for their specific sites on DNA: the role of DNA conformation. Biophysical journal 90, 2731 (Apr 15, 2006).

19. A. Turkin, A. M. van Oijen, A. A. Turkin, Theory of bimolecular reactions in a solution with linear traps: Application to the problem of target search on DNA. Phys Rev E 92, (Nov 3, 2015).

20. A. Turkin et al., Speeding up biomolecular interactions by molecular sledding. Chemical Science, (2016).

21. L. Unterholzner, A. G. Bowie, Innate DNA sensing moves to the nucleus. Cell host & microbe 9, 351 (May 19, 2011).

22. M. H. Orzalli, S. E. Conwell, C. Berrios, J. A. DeCaprio, D. M. Knipe, Nuclear interferon-inducible protein 16 promotes silencing of herpesviral and transfected DNA. Proc Natl Acad Sci U S A 110, E4492 (Nov 19, 2013).

23. K. E. Johnson et al., IFI16 Restricts HSV-1 Replication by Accumulating on the HSV-1 Genome, Repressing HSV-1 Gene Expression, and Directly or Indirectly Modulating Histone Modifications. PLoS pathogens 10, e1004503 (Nov, 2014).

24. J. D. McGhee, J. M. Nickol, G. Felsenfeld, D. C. Rau, Higher order structure of chromatin: orientation of nucleosomes within the 30 nm chromatin solenoid is independent of species and spacer length. Cell 33, 831 (Jul, 1983).

25. T. Li, J. Chen, I. M. Cristea, Human cytomegalovirus tegument protein pUL83 inhibits IFI16-mediated DNA sensing for immune evasion. Cell host & microbe 14, 591 (Nov 13, 2013).

26. K. M. Monroe et al., IFI16 DNA sensor is required for death of lymphoid CD4 T cells abortively infected with HIV. Science 343, 428 (Jan 24, 2014).

27. K. Luger, T. J. Rechsteiner, T. J. Richmond, Expression and purification of recombinant histones and nucleosome reconstitution. Methods Mol Biol 119, 1 (1999).

28. N. A. Tanner, A. M. van Oijen, Visualizing DNA replication at the single-molecule level. Methods in enzymology 475, 259 (2010).

29. A. Tafvizi et al., Tumor suppressor p53 slides on DNA with low friction and high stability. Biophysical journal 95, L01 (Jul, 2008).

30. A. Tafvizi, F. Huang, A. R. Fersht, L. A. Mirny, A. M. van Oijen, A single-molecule characterization of p53 search on DNA. Proc Natl Acad Sci U S A 108, 563 (Jan 11, 2011).

31. J. S. Leith et al., Sequence-dependent sliding kinetics of p53. Proc Natl Acad Sci U S A 109, 16552 (Oct 9, 2012).